

# Quantum simulation of Heisenberg spin chains with next nearest neighbor interactions in coupled cavities

Zhi-Xin Chen, Zheng-Wei Zhou,\* Xingxiang Zhou,† Xiang-Fa Zhou, and Guang-Can Guo  
*Key Laboratory of Quantum Information, University of Science and Technology of China,  
Chinese Academy of Sciences, Hefei, Anhui 230026, China*

We propose a scheme to simulate one-dimensional XXZ-type Heisenberg spin models with competing interactions between nearest-neighbors (NNs) and next-NNs in photon-coupled micro-cavities. Our scheme, for the first time, exploits the rich resources and flexible controls available in such a system to realize arbitrarily adjustable ratios between the effective NN and next-NN coupling strengths. Such powerful capability allows us to simulate frustration phenomena and disorder behaviors in 1-d systems arising from next-NN interactions, a large class of problems of great importance in condensed matter physics. Our scheme is robust due to the lack of atomic excitations which suppresses spontaneous emission and cavity decay strongly.

PACS numbers: 03.67.Mn, 42.50.Vk, 75.10.Jm

Quantum simulation is an important application of quantum information science. As a promising physical system for quantum simulation, ultracold atoms trapped in an optical lattice [1, 2] have many appealing properties such as long coherence times, the possibility of simultaneous initialization of a large number of particles, and tunable effective coupling strength within a large range. However, it is difficult to focus a laser beam on a single atom due to the short optical lattice period which makes it challenging to realize single-site operations [3]. To address this challenge, recently arrays of photon-coupled microcavities have been suggested as an alternative quantum simulator [4–19]. An artificial system on a micro-chip, microcavities can be fabricated in desired structures and dimensions with great precision, a significant advantage that allows to realize both single-site operations and neighboring-sites interactions easily [4].

In previous research on quantum simulation, the focus has been on realizing various spin models with on-site and NN interactions, the most widely used model in studies of condensed-matter physics problems such as quantum magnetism [20, 21]. For instance, it was demonstrated that an array of coupled cavities with one atom in each cavity can be used to simulate the anisotropic (XYZ) Heisenberg spin- $\frac{1}{2}$  model. It was further shown that the XXZ-type Heisenberg spin model of any high spin can be realized using a cavity array with a number of atoms in each cavity [9]. The XXZ-type Heisenberg spin model can also be realized when the spin states are represented by polaritons [10, 11]. Much of the recent research was reviewed in [4]. However, it is well known in condensed-matter physics that many important physics and exotic phenomena arise due to the long-range nature of interactions between spins. A particularly important model to capture this is a spin model with both (and possibly competing) NN and next-NN interactions, which is known to reveal many important physics such as Tomonaga-Luttinger liquid states and spin-Peierls states [21–23]. It is even suggested that it could be used to study the mechanism for iron-based superconductors [24]. The importance of such frustrated spin systems has also been recognized in the context of quantum information. For instance, behavior of quantum entanglement in frustrated spin systems was studied by a number of authors [25–29] and interesting and deep connections between entanglement and phase transitions were discovered in these systems. Unfortunately, physical implementation for a spin-chain quantum simulator with both tunable NN and next-NN interactions has not been available, mainly due to the technical difficulty in realizing controllable next-NN interactions. For instance, in ultracold atomic systems the adjustable spin interactions are usually realized by controlling the wave function overlap between neighboring sites. This technique is not useful in engineering next-NN interactions since the wavefunction overlap falls off exponentially with distance.

In this work, we show how one can implement an effective spin model in a microcavity system with both NN and next-NN interactions. By taking advantage of the many controls available and using a smart idea of interaction cancellation and enhancement, we can adjust at will the ratio between the NN and next-NN interaction strengths. This then allows for the first time to simulate a large class of condensed-matter physics problems in which the competition between NN and next-NN interactions plays an essential role. Moreover, in our approach, cavity field is always kept in ground state and atoms remain in two long-lived states. Since excited atomic levels and cavity photon modes only appear in virtual processes, spontaneous emission of internal states and cavity decay are strongly suppressed.

We consider an array of cavities that are coupled via exchange of photons with one 4-level atom in each cavity

---

\*Electronic address: zwzhou@ustc.edu.cn

†Electronic address: xizhou@ustc.edu.cn

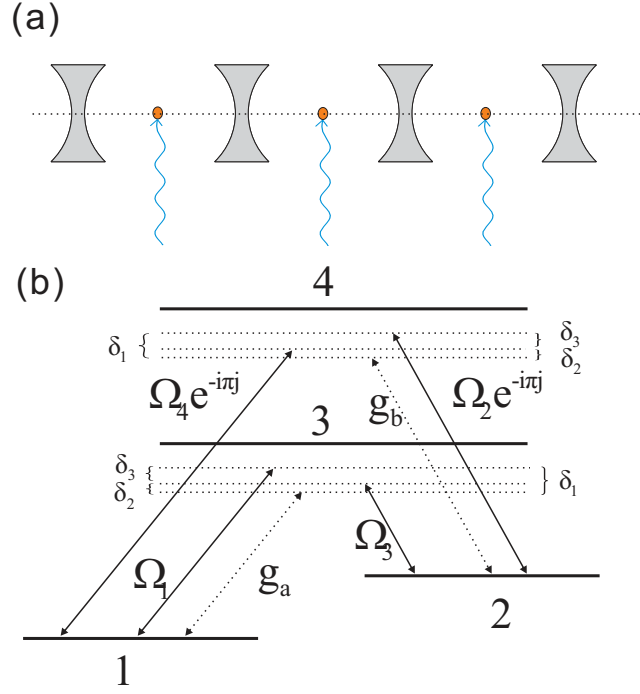


FIG. 1: (color online). (a) A one-dimensional array of coupled cavities with one 4-level atom in each cavity. (b) Involved atomic levels and transitions.

(Fig.1). Such a model can be realized in several kinds of physical systems such as microtoroidal cavity arrays [17], photonic crystal defects [18] and superconducting stripline resonators [19]. Two long-lived levels,  $|1\rangle$  and  $|2\rangle$ , represent the two spin states  $|\downarrow\rangle$  and  $|\uparrow\rangle$  for the effective spin. Together with two excited states  $|3\rangle$  and  $|4\rangle$ , they form two independent  $\Lambda$  level structures. We denote the subsystem consisting of levels  $|1\rangle$ ,  $|2\rangle$ , and  $|3\rangle$   $\Lambda_a$ , and that consisting of  $|1\rangle$ ,  $|2\rangle$ , and  $|4\rangle$   $\Lambda_b$ .

In previous research, a simpler atomic level configuration with one  $\Lambda$  structure was used to realize effect spin models with NN XXZ interactions [8, 9]. In these models, interaction strength between spins decreases rapidly with distances and next-NN interactions are negligibly small compared to NN interactions. In our study, by cleverly adjusting relevant experimental conditions, we can make interactions arising due to the two independent level structures  $\Lambda_a$  and  $\Lambda_b$  add up or cancel each other depending on the phases of the control lasers. This is the key idea that allows us to realize arbitrary ratios between NN and next-NN interaction strengths.

We now derive the effective Hamiltonian of the photon coupled microcavity system in Fig. 1 (a) when each atom couples with two cavity modes and four external lasers (Fig.1(b)). Suppose two cavity modes,  $\omega_a$  and  $\omega_b$ , are close in energy to the transitions  $|1\rangle \leftrightarrow |3\rangle$  and  $|2\rangle \leftrightarrow |4\rangle$ , and thus drive these two transitions with strengths  $g_a$  and  $g_b$  respectively. Further, we apply four lasers with frequencies  $\omega_1$ ,  $\omega_2$ ,  $\omega_3$  and  $\omega_4$  to drive the transitions  $|1\rangle \leftrightarrow |3\rangle$ ,  $|2\rangle \leftrightarrow |4\rangle$ ,  $|2\rangle \leftrightarrow |3\rangle$  and  $|1\rangle \leftrightarrow |4\rangle$ , with Rabi frequencies  $\Omega_1$ ,  $\Omega_2 e^{-i\pi j}$ ,  $\Omega_3$ ,  $\Omega_4 e^{-i\pi j}$  (the index  $j$  represents the  $j$ th cavity), respectively (without loss of generality, here, assume all the  $\Omega_i$  are real). Here, we have modulated the phases of lasers  $\omega_2$  and  $\omega_4$  on purpose, and as will be seen later this phase modulation plays a key role in our scheme. All the transitions are assumed to be large detuned, i.e., the magnitudes of the detunings  $\delta_{31} = \omega_{31} - \omega_a$ ,  $\delta_{42} = \omega_{42} - \omega_b$ ,  $\Delta_{31} = \omega_{31} - \omega_1$ ,  $\Delta_{42} = \omega_{42} - \omega_2$ ,  $\Delta_{32} = \omega_{32} - \omega_3$ , and  $\Delta_{41} = \omega_{41} - \omega_4$  ( $\omega_{\mu\nu}$  is the energy difference between level  $|\mu\rangle$  and  $|\nu\rangle$ ) are much greater than the transition strengths  $|g_a|$ ,  $|g_b|$  and  $|\Omega_i|$  ( $i = 1, 2, 3, 4$ ). Under these conditions, in the rotating frame, we can perform a standard adiabatic elimination of the atomic excited states  $|3\rangle$  and  $|4\rangle$  [30] and obtain an effective Hamiltonian

$$\begin{aligned}
H = & - \sum_j [A_1|1_j\rangle\langle 1_j|a_j e^{i\delta_1 t} + A_2|2_j\rangle\langle 1_j|a_j e^{i\delta_2 t} + H.c.] \\
& - \sum_j [(-1)^j B_1|2_j\rangle\langle 2_j|b_j e^{i\delta_1 t} + (-1)^j B_2|1_j\rangle\langle 2_j|b_j e^{i\delta_2 t} + H.c.] \\
& - \sum_j [(A_3|1_j\rangle\langle 2_j| + B_3|2_j\rangle\langle 1_j|)e^{i\delta_3 t} + H.c.] \\
& - \sum_j [(\frac{\Omega_1^2}{\Delta_{31}} + \frac{\Omega_4^2}{\Delta_{41}})|1_j\rangle\langle 1_j| + (\frac{\Omega_3^2}{\Delta_{32}} + \frac{\Omega_2^2}{\Delta_{42}})|2_j\rangle\langle 2_j|] \\
& - \sum_j (\frac{g_a^2}{\delta_{31}}|1_j\rangle\langle 1_j|a_j^\dagger a_j + \frac{g_b^2}{\delta_{42}}|2_j\rangle\langle 2_j|b_j^\dagger b_j) \\
& + \sum_j [J_a(a_j^\dagger a_{j+1} + a_j a_{j+1}^\dagger) + J_b(b_j^\dagger b_{j+1} + b_j b_{j+1}^\dagger)],
\end{aligned} \tag{1}$$

where  $\delta_1 = \delta_{31} - \Delta_{31} = \delta_{42} - \Delta_{42}$ ,  $\delta_2 = \delta_{31} - \Delta_{32} = \delta_{42} - \Delta_{41}$ , and  $\delta_3 = \delta_1 - \delta_2$  are the two-photon detunings,  $A_1 = \frac{\Omega_1 g_a}{2}(\frac{1}{\Delta_{31}} + \frac{1}{\delta_{31}})$ ,  $A_2 = \frac{\Omega_3 g_a}{2}(\frac{1}{\Delta_{32}} + \frac{1}{\delta_{31}})$ ,  $A_3 = \frac{\Omega_1 \Omega_3}{2}(\frac{1}{\Delta_{31}} + \frac{1}{\Delta_{32}})$ ,  $B_1 = \frac{\Omega_2 g_b}{2}(\frac{1}{\Delta_{42}} + \frac{1}{\delta_{42}})$ ,  $B_2 = \frac{\Omega_4 g_b}{2}(\frac{1}{\Delta_{41}} + \frac{1}{\delta_{42}})$ , and  $B_3 = \frac{\Omega_2 \Omega_4}{2}(\frac{1}{\Delta_{41}} + \frac{1}{\Delta_{42}})$  are the effective coupling strengths,  $J_a$ ,  $J_b$  are the tunnelling rate of photons between neighboring cavities(all assumed to be real). Notice that the effective interaction strengths  $A_1$  and  $A_2$  are induced by the level structure  $\Lambda_a$ , whereas  $B_1$  and  $B_2$  arise due to  $\Lambda_b$ , and there is a phase factor of  $(-1)^j$  from the Rabi frequencies  $\Omega_2 e^{-i\pi j}$  and  $\Omega_4 e^{-i\pi j}$  in the  $j$ th cavity.

We can now derive the effective spin interactions using the virtual-transition induced by effective Hamiltonian in Eq. (1). To avoid excitations of real photons and ensure that all two-photon transitions are independent when we derive the effective spin Hamiltonian [9], we further require that all two-photon transitions be large detuned, i.e.,  $|\delta_i|$ ,  $|\delta_3 - \delta_2| \gg |A_i|$ ,  $|B_i|$ ,  $|J_a|$ ,  $|J_b|$ ,  $|\frac{g_a^2}{\delta_{31}}|$ ,  $|\frac{g_b^2}{\delta_{42}}|$  ( $i=1,2,3$ ). We define the spin operators  $S_j^z = \frac{1}{2}(|2_j\rangle\langle 2_j| - |1_j\rangle\langle 1_j|)$ ,  $S_j^+ = |2_j\rangle\langle 1_j|$ ,  $S_j^- = |1_j\rangle\langle 2_j|$ . Before proceeding, we simplify the Hamiltonian in Eq. (1). First, when we consider the third term up to second order, it is  $\sum_j \frac{2}{\delta_3}(B_3^2 - A_3^2)S_j^z$ , so the third term and the fourth term only contribute to effective local magnetic field. We temporarily neglect them. Second, the fifth term is a perturbation term that modifies the detunings of the two-photon transitions, i.e.,  $\delta_{a1} = \delta_1 + \frac{g_a^2}{\delta_{31}}$ ,  $\delta_{a2} = \delta_2 + \frac{g_a^2}{\delta_{31}}$ ,  $\delta_{b1} = \delta_1 + \frac{g_b^2}{\delta_{42}}$ ,  $\delta_{b2} = \delta_2 + \frac{g_b^2}{\delta_{42}}$ . Finally, we assume periodic boundary conditions and take advantage of Fourier transformation to diagonalize the photon coupling terms. Defining  $a_j$  ( $b_j$ ) =  $\frac{1}{\sqrt{N}} \sum_{k=1}^N F_{jk} c_k$  ( $d_k$ ), where  $N$  is the total number of the cavities,  $F_{jk} = \exp(-i\frac{2\pi}{N}jk)$  and  $\sum_{j=1}^N F_{jk}^* F_{jl} = N\delta_{kl}$  ( $\delta_{kl}$  is the Kronecker function), we have

$$\sum_j J_a(a_j^\dagger a_{j+1} + a_j a_{j+1}^\dagger) = \sum_k T_{ak} c_k^\dagger c_k, \tag{2}$$

$$\sum_j J_b(b_j^\dagger b_{j+1} + b_j b_{j+1}^\dagger) = \sum_k T_{bk} d_k^\dagger d_k, \tag{3}$$

where  $T_{ak} = J_a \sum_{j,l} \frac{1}{N}(F_{jk}^* F_{j+1,l} + F_{jk} F_{j+1,l}^*) = 2J_a \cos(\frac{2\pi}{N}k)$  and  $T_{bk} = 2J_b \cos(\frac{2\pi}{N}k)$ . The Hamiltonian in the rotating frame reads

$$\begin{aligned}
H = & - \sum_{j,k} \{ [A_1(\frac{1}{2}I_j - S_j^z)e^{i\delta_{a1}t} + A_2 S_j^+ e^{i\delta_{a2}t}] \frac{F_{jk}}{\sqrt{N}} c_k e^{-iT_{ak}} + H.c. \} \\
& - \sum_{j,k} \{ (-1)^j [B_1(\frac{1}{2}I_j + S_j^z)e^{i\delta_{b1}t} + B_2 S_j^- e^{i\delta_{b2}t}] \frac{F_{jk}}{\sqrt{N}} d_k e^{-iT_{bk}} + H.c. \}.
\end{aligned} \tag{4}$$

When the large detuning conditions  $|\delta_{ai}|$ ,  $|\delta_{bi}|$ ,  $|\delta_{a1} - \delta_{a2}|$ ,  $|\delta_{b1} - \delta_{b2}| \gg |A_i|$ ,  $|B_i|$ ,  $|J_a|$ ,  $|J_b|$  are satisfied, all terms are independent when we adiabatically eliminate the photon states, and we obtain the effective spin Hamiltonian

$$\begin{aligned}
H = & \sum_{j,l,k} \left[ \frac{1}{N} \frac{F_{jk} F_{lk}^*}{\delta_{a1} - T_{ak}} A_1^2 \left( \frac{1}{2} I_j - S_j^z \right) \left( \frac{1}{2} I_l - S_l^z \right) + \frac{1}{N} \frac{F_{jk} F_{lk}^*}{\delta_{a2} - T_{ak}} A_2^2 S_j^+ S_l^- \right] \\
& + \sum_{j,l,k} (-1)^{j+l} \left[ \frac{1}{N} \frac{F_{jk} F_{lk}^*}{\delta_{b1} - T_{bk}} B_1^2 \left( \frac{1}{2} I_j + S_j^z \right) \left( \frac{1}{2} I_l + S_l^z \right) + \frac{1}{N} \frac{F_{jk} F_{lk}^*}{\delta_{b2} - T_{bk}} B_2^2 S_j^- S_l^+ \right].
\end{aligned} \tag{5}$$

It is clear from Eq. (5) that effective spin interactions arise between any pair of lattice sites  $j$  and  $l$  due to nonlocal modes  $c_k$  and  $d_k$ . However, due to the large detuning conditions  $|\delta_{\mu i}| \gg |T_{\mu k}| = |2J_{\mu} \cos(\frac{2\pi}{N}k)|$  ( $\mu = a, b; i = 1, 2$ ), the interaction strength drops quickly with the site distance  $|i - j|$ . To see this, we expand the following term for interaction strengths in Eq. (5) to second order in  $T_{\mu k}/\delta_{\mu i}$ . Making use of the relations  $\sum_k F_{jk} F_{lk}^* = N\tilde{\delta}_{jl}$ ,  $\sum_k F_{jk} F_{lk}^* \cdot 2\cos(\frac{2\pi}{N}k) = N(\tilde{\delta}_{j,l+1} + \tilde{\delta}_{j+1,l})$ ,  $\sum_k F_{jk} F_{lk}^* \cdot (2\cos(\frac{2\pi}{N}k))^2 = N(2\tilde{\delta}_{jl} + \tilde{\delta}_{j,l+2} + \tilde{\delta}_{j+2,l})$ , we obtain

$$\begin{aligned}
\frac{1}{N} \sum_k \frac{F_{jk} F_{lk}^*}{\delta_{\mu i} - T_{\mu k}} & \approx \frac{1}{N} \sum_k \frac{F_{jk} F_{lk}^*}{\delta_{\mu i}} \left( 1 + \frac{T_{\mu k}}{\delta_{\mu i}} + \frac{T_{\mu k}^2}{\delta_{\mu i}^2} \right) \\
& = \frac{1}{\delta_{\mu i}} \left( 1 + \frac{2J_{\mu}^2}{\delta_{\mu i}^2} \right) \tilde{\delta}_{j,l} + \frac{J_{\mu}}{\delta_{\mu i}^2} (\tilde{\delta}_{j,l+1} + \tilde{\delta}_{j+1,l}) + \frac{J_{\mu}^2}{\delta_{\mu i}^3} (\tilde{\delta}_{j,l+2} + \tilde{\delta}_{j+2,l}).
\end{aligned} \tag{6}$$

Substituting the expanded terms in Eq. (5), we obtain the following effective spin Hamiltonian to second order in  $J_{\mu}/\delta_{\mu i}$ :

$$\begin{aligned}
H = & \sum_j \left\{ 2 \left[ \frac{J_a}{\delta_{a1}^2} A_1^2 + (-1)^1 \frac{J_b}{\delta_{b1}^2} B_1^2 \right] S_j^z S_{j+1}^z \right. \\
& + \left[ \frac{J_a}{\delta_{a2}^2} A_2^2 + (-1)^1 \frac{J_b}{\delta_{b2}^2} B_2^2 \right] (S_j^+ S_{j+1}^- + S_j^- S_{j+1}^+) \\
& + 2 \left[ \frac{J_a^2}{\delta_{a1}^3} A_1^2 + (-1)^2 \frac{J_b^2}{\delta_{b1}^3} B_1^2 \right] S_j^z S_{j+2}^z \\
& + \left[ \frac{J_a^2}{\delta_{a2}^3} A_2^2 + (-1)^2 \frac{J_b^2}{\delta_{b2}^3} B_2^2 \right] (S_j^+ S_{j+2}^- + S_j^- S_{j+2}^+) \\
& \left. + h_j S_j^z \right\},
\end{aligned} \tag{7}$$

where  $h_j$  is the strength of local effective magnetic field [31]. It can be seen from Eq. (7) that the effective spin interaction strength terms proportional to  $A_i$  and  $B_i$  arise from the atom's level structures  $\Lambda_a$  and  $\Lambda_b$  separately. For both  $\Lambda_a$  and  $\Lambda_b$ , the next-NN interaction strength is 1 order of magnitude (in  $J/\delta$ ) smaller than that of NN interaction. Therefore, if only one of the level structures  $\Lambda_a$  and  $\Lambda_b$  was present, it can be seen from the above Hamiltonian that the next-NN interaction would have been negligibly weak compared to NN interaction because their ratio is  $J_{\mu}/\delta_{\mu i} \ll 1$ . For this reason, the next-NN interactions are omitted in previous work [8, 9]. However, in our system both level structures  $\Lambda_a$  and  $\Lambda_b$  contribute to the effective spin interactions. When calculating the total effective interaction strength, we see that contributions due to  $\Lambda_a$  and  $\Lambda_b$  tend to cancel for NN interactions but add up for next-NN interactions, due to our careful choice of the control laser phases. By using this smart idea of interaction cancellation and enhancement, we can arbitrarily adjust the ratio between NN and next-NN interaction strengths. Finally, we simplify the above effective spin Hamiltonian and write it in the following form

$$H = \sum_j \left[ \left[ \sum_{\sigma=1,2} J_{\sigma} (S_j^x S_{j+\sigma}^x + S_j^y S_{j+\sigma}^y) + \lambda_{\sigma} S_j^z S_{j+\sigma}^z \right] + h_j S_j^z \right]. \tag{8}$$

Here, the effective coupling strengths are  $J_1 = 2(\frac{J_a}{\delta_{a2}^2} A_2^2 - \frac{J_b}{\delta_{b2}^2} B_2^2)$ ,  $J_2 = 2(\frac{J_a^2}{\delta_{a2}^3} A_2^2 + \frac{J_b^2}{\delta_{b2}^3} B_2^2)$ ,  $\lambda_1 = 2(\frac{J_a}{\delta_{a1}^2} A_1^2 - \frac{J_b}{\delta_{b1}^2} B_1^2)$ ,  $\lambda_2 = 2(\frac{J_a^2}{\delta_{a1}^3} A_1^2 + \frac{J_b^2}{\delta_{b1}^3} B_1^2)$ .

The interaction cancellation and enhancement is clearly reflected in the above expressions for  $J_1$  and  $J_2$ , effective interaction strengths between NN and next-NN spins in the Hamiltonian Eq. (8). Obviously, by choosing close values for  $\frac{J_a}{\delta_{a1}^2} A_1^2$  and  $\frac{J_b}{\delta_{b2}^2} B_2^2$  ( $i = 1, 2$ ), we can make  $J_2$  comparable to or even greater than  $J_1$ . We can also adjust the relative signs of  $J_1$  and  $J_2$  easily.

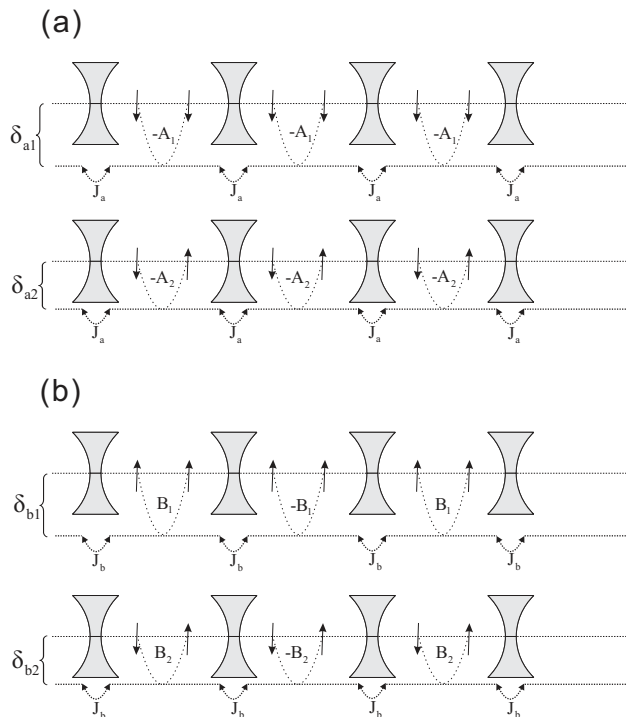


FIG. 2: Atoms in cavities interact via exchange of virtual photons of cavity modes  $\omega_a$  ((a)) and  $\omega_b$  ((b)). The two spin states  $|\downarrow\rangle$  and  $|\uparrow\rangle$  are represented by two long-lived atomic levels  $|1\rangle$  and  $|2\rangle$ .  $A_i$ ,  $B_i$  ( $i = 1, 2$ ) are the effective coupling strengths,  $\delta_{ai}$ ,  $\delta_{bi}$  are the detunings,  $J_a$ ,  $J_b$  are the tunnelling rates of photons between neighboring cavities.

To gain a better intuitive understanding of the critical role that interaction cancellation and enhancement plays in the physics underlying the effective Hamiltonian in Eq. (8), we present a simple physical picture in Fig.2. Fig. 2 (a) describes interactions induced by the two-photon transitions of the  $\Lambda_a$  level structure. In this process, atoms interact via the exchange of virtual photons of the cavity mode  $\omega_a$ . Similarly, Fig.2(b) describes interactions induced by the two-photon transitions of the  $\Lambda_b$  level structure, where atoms interact via the exchange of virtual photons of the cavity mode  $\omega_b$ . The difference is, due to the phase modulation of the control lasers, in Fig.2(b), the amplitude of emitting or absorbing a photon is site-dependent, i.e.,  $(-1)^{j+1}B_i$  ( $i = 1, 2$ ) in the  $j$ th cavity.

Now, we consider the first case in Fig.2(a), which generates ZZ interactions. The probability amplitude that the first atom emits a virtual photon with frequency  $\omega_a$  is  $\frac{J_a}{\delta_{a1}}$ , where  $\delta_{a1}$  is the detuning. Then the photon tunnels to the second cavity with amplitude  $\frac{J_a}{\delta_{a1}}$ . If it is absorbed with amplitude  $(-A_1)$ , the strength of NN interaction is  $\frac{-A_1}{\delta_{a1}} \frac{J_a}{\delta_{a1}} (-A_1) = \frac{J_a}{\delta_{a1}^2} A_1^2 > 0$ . The photon can further tunnel to the third cavity with probability amplitude  $\frac{J_a}{\delta_{a1}}$ , and be absorbed with amplitude  $(-A_1)$ . This results in a next-NN interaction with strength  $\frac{-A_1}{\delta_{a1}} \frac{J_a}{\delta_{a1}} \frac{J_a}{\delta_{a1}} (-A_1) = \frac{J_a^2}{\delta_{a1}^3} A_1^2 > 0$ . In Fig.2(a), similar processes occur and they can be understood by replacing  $A_1$  and  $\delta_{a1}$  with  $A_2$  and  $\delta_{a2}$  in the above discussion. It generates XX interactions. In Fig.2(b), due to the site-dependent modulation of the phases of the laser  $\omega_2$  and  $\omega_4$ , the NN sites have different amplitudes,  $B_i$  and  $(-B_i)$  ( $i = 1, 2$ ). So the effective couplings of the NN and next-NN interactions are  $\frac{B_i}{\delta_{bi}} \frac{J_b}{\delta_{bi}} (-B_i) = -\frac{J_b}{\delta_{bi}^2} B_i^2 < 0$  and  $\frac{B_i}{\delta_{bi}} \frac{J_b}{\delta_{bi}} \frac{J_b}{\delta_{bi}} B_i = \frac{J_b^2}{\delta_{bi}^3} B_i^2 > 0$ , respectively. All the effective couplings have a factor of 2 because the atoms that emit and absorb the virtual photon can be switched. We can clearly see that the total interactions of the next-NN sites enhance while the total interactions of the NN sites cancel, leading to the effective Hamiltonian in Eq. (8).

It should be noticed that the effective Hamiltonian in Eq. (8) is highly tunable, because it is determined by 6 free parameters (2 parameters on frequency detuning and 4 parameters on intensity of control laser). As long as the large detuning conditions are satisfied, the interaction strengths in effective Hamiltonian Eq. (8) can be adjusted at will allowing to realize arbitrary ratios between  $J_1/J_2$  and  $\lambda_1/\lambda_2$ . With its large realizable parameter space, it is then convenient to use this model to simulate a large class of XXZ Heisenberg spin chain problems in which competing interactions between NN and next-NN play an essential role.

As an example, we discuss how our system can be used to simulate frustration phenomena in 1d condensed matter physics. By introducing a new stark shift[8], the effective local magnetic field can be set to 0. When we choose system

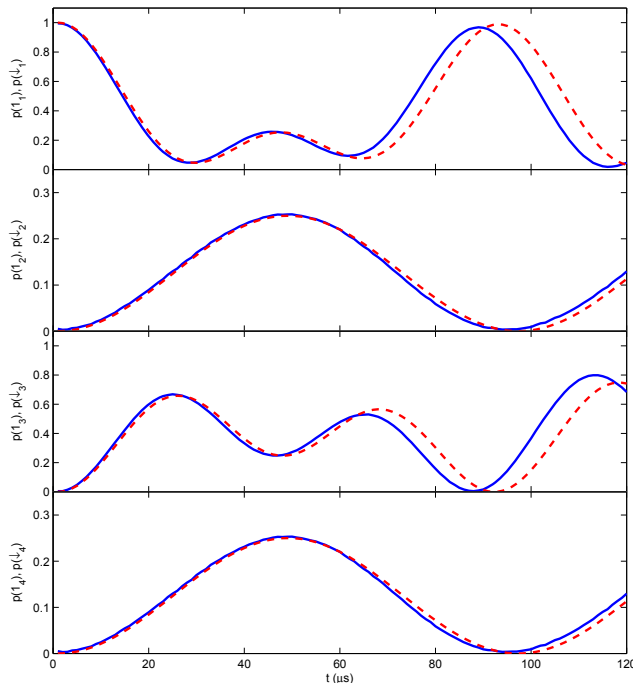


FIG. 3: (color online). Time evolution of occupation probability  $p(1_j)$  of state  $|1_j\rangle$  ( $j = 1, 2, 3, 4$ ), calculated using the full Hamiltonian (solid blue line) and effective spin Hamiltonian (dashed red line), for parameters  $A_1 = A_2 = 0.1$  GHz,  $B_1 = B_2 = 0.096$  GHz,  $A_3 = B_3 = 0.02$  GHz,  $\delta_1 = 4$  GHz,  $\delta_2 = 3$  GHz,  $\delta_3 = 1$  GHz,  $g_a^2/\delta_{31} = g_b^2/\delta_{42} = 0.1$  GHz, and  $J_a = J_b = 0.2$  GHz.

parameters such that  $J_2 = \lambda_2 > 0$  and  $J_1 > 0$ ,  $\lambda_1 > 0$ , the Hamiltonian  $H$  is the well-known anisotropic Heisenberg model with competing interactions (“frustration”) originally studied by Haldane [22]. Haldane predicted four phases for this system at zero temperature: spin fluid phase, Néel phase, dimer phase, and bound phase. When the ratio of  $J_2/J_1$  is increased, the interesting phenomenon of spontaneous dimerization takes place.

In coupled cavities systems, addressing of individual cavities is available. Therefore, one can also simulate a frustrated spin chain with disorder. Yusuf et. al. predicted the random singlet phase and the large spin phase in random antiferromagnetic spin-1/2 chains with NN and next-NN couplings. A strong next-NN coupling will drive the system to a large spin phase [32].

Aside from simulating frustrated spin problems of interests in the conventional context of condensed matter physics, our system with both tunable NN and next-NN interactions is also very valuable for quantum information studies. Spin chains with NN interactions are known to be useful for various quantum information tasks. For instance, they can be used to transfer quantum states [33]. Whether a spin chain with both NN and next-NN interactions can transfer quantum states more efficiently is an interesting topic to investigate, and our system provides a physical implementation for such a system readily. Perhaps more intriguingly, our system offers a powerful quantum simulation tool to study the deep connections between quantum entanglement and phase transitions in frustrated spin systems. This important subject has been discussed theoretically [26–29], however no physical implementation of such a system with controllable NN and next-NN interaction strengths was available to check the findings in these preliminary theoretical research. Our system for the first time makes it possible to physically simulate relevant frustrated spin models. Because of the large realizable parameter space and ability to address individual spins in our system, we can simulate a large class of phase transitions and also study detailed information on entanglement in the system. This then allows to verify previous results on entanglement and phase transitions in frustrated spin systems and also simulate more complicated problems beyond the reach of conventional numerical methods.

Our derivation of the effective spin Hamiltonian in Eq. (8) involves a large number of assumptions and approximations. To check the validity of these approximations and the accuracy of the results, we numerically simulate the dynamics generated by the full Hamiltonian in Eq. (1) and the effective model described by Eq. (8) and compare the results.

As an example, we consider four atoms in four cavities, initially in the state  $|1_1\rangle \otimes |2_2\rangle \otimes |2_3\rangle \otimes |2_4\rangle$  corresponding to a spin state where only one spin points down,  $|\downarrow\uparrow\uparrow\uparrow\rangle$ . We calculate the time evolution of the probability of atom

$j$  in the  $|1\rangle$  state, i.e., the occupation probability  $p(1_j)$  of state  $|1_j\rangle$  ( $j = 1, 2, 3, 4$ ) using the full Hamiltonian in Eq. (1). This corresponds to the probability of spin  $j$  pointing down,  $p(\downarrow_j)$ , which we calculate using the effective spin Hamiltonian in Eq. (8). Fig.3 shows  $p(1_j)$  and  $p(\downarrow_j)$  for an effective Hamiltonian(8) with  $J_1 = 0.0326\text{MHz}$ ,  $J_2 = 0.0516\text{MHz}$ ,  $\lambda_1 = 0.0187\text{MHz}$  and  $\lambda_2 = 0.0223\text{MHz}$  [34]. To demonstrate the high tunability of our model, we have deliberately chosen the system parameters such that next-NN interactions are stronger than NN interactions. Due to periodic boundary conditions, the results of  $p(1_2)$  and  $p(1_4)$  are the same. As shown in Fig. 3, the numerical results of the Hamiltonian Eq. (1) and those of the effective model agree with each other reasonably well. Therefore, our effective model is valid.

Quantum simulation based on our effective spin model is adversely affected by nonidealities in the system, most notably the cavity decay and limited lifetime of the excited atomic states. To reliably observe exchange dynamics due to next-NN interactions, the coupling strengths  $J_\sigma$  and  $\lambda_\sigma$  should be at least one or two orders of magnitude larger than the cavity decay rates and the lifetimes of the atomic upper levels. Defining  $\Omega = \max(\Omega_1, \Omega_2, \Omega_3, \Omega_4)$ ,  $g = \max(g_a, g_b)$ ,  $J = \max(J_a, J_b)$ ,  $\Delta = \min(\Delta_{31}, \Delta_{32}, \Delta_{41}, \Delta_{42})$ , and  $\delta = \min(\delta_1, \delta_2)$ , one can see that the mean population of the atomic excited state  $|3\rangle$  (or  $|4\rangle$ ) can be approximately written as  $|\Omega/\Delta|^2$ . This results in an effective decay rate  $|\Omega/\Delta|^2\Gamma_E$  with  $\Gamma_E$  the linewidth of the upper level. Similarly, the effective cavity field decay rate can be expressed as  $|\Omega g/(\Delta\delta)|^2\Gamma_C$ , where  $\Gamma_C$  describes the cavity decay of photons [35]. Since the coupling  $J_\sigma$  and  $\lambda_\sigma$  is approximately  $4J^2\Omega^2g^2/(\Delta^2\delta^3)$ , this leads to the constraints  $\Gamma_E \ll 4g^2J^2/\delta^3$  and  $\Gamma_C \ll 4J^2/\delta$ . Without loss of generality, we assume  $\delta > 2J$  with  $2J$  the bandwidth of the photons in the cavity array. Thus, to ensure that the photons tunnel between cavities before they decay, the condition  $\Gamma_C \ll J$  must be satisfied. Additionally, for  $\Gamma_E \ll 4g^2J^2/\delta^3$ , high cooperativity factors  $g^2/(\Gamma_C\Gamma_E)$  and high ratios of coupling to dissipation  $g/\Gamma_E$  are favorable.

Experimentally, the requirements on parameters discussed above can be fulfilled in microcavities with high quality factors. For toroidal microcavities in [17], the predicted critical atom number can approach  $10^{-7}$ , which results in a cooperativity factor  $g^2/(\Gamma_C\Gamma_E) \sim 10^7$  and a ratio  $g/\Gamma_E \sim 10^3$ . For a strongly coupled single quantum dot-cavity system [18],  $g \simeq 20\text{GHz}$  can be achieved with  $\Gamma_C = 24\text{GHz}$  and  $\Gamma_E = 18\text{MHz}$ , for which we have  $g^2/(\Gamma_C\Gamma_E) \sim 10^3$  and  $g/\Gamma_E \sim 10^3$ . In both systems, the photons can transfer between different cavities via their evanescent fields or optical fibres. Thus, our effective spin model with next-NN interactions can be readily and reliably realized in presently available systems.

In this work, we have shown that one dimensional frustrated spin models can be simulated using atoms in photon coupled cavities. By choosing the phases of control lasers appropriately, it is possible to make interactions arising from different level structures add up or cancel each other, which then allows to adjust the ratio between NN and next-NN interaction strengths at will. Quantum simulation using our system is robust and reliable since the atoms are only virtually excited and no real photon absorption and generation are involved and thus dissipative processes such as photon decay and spontaneous emission are strongly suppressed.

This work was funded by National Fundamental Research Program (2006CB921900), the Innovation funds from Chinese Academy of Sciences, and National Natural Science Foundation of China (Grant No. 60621064, No. 10874170, No. 10875110, and No. 60836001). Z.-W. Zhou gratefully acknowledges the support of K.C.Wong Education Foundation, Hong Kong.

- 
- [1] D. Jaksch, C. Bruder, J. I. Cirac, C. W. Gardiner, and P. Zoller, Phys. Rev. Lett. **81**, 3108 (1998).
  - [2] M. Greiner, O. Mandel, T. Esslinger, T. W. Hönsch, and I. Bloch, Nature (London) **415**, 39 (2002).
  - [3] T. Calarco, U. Dorner, P. Julienne, C. Williams, and P. Zoller, Phys. Rev. A **70**, 012306 (2004); K. G. H. Vollbrecht, E. Solano, and J. I. Cirac, Phys. Rev. Lett. **93**, 220502 (2004); J. Joo, Y. L. Lim, A. Beige, and P. L. Knight, Phys. Rev. A **74**, 042344 (2006); C. Zhang, S. L. Rolston, and S. D. Sarma, Phys. Rev. A **74**, 042316 (2006); Z. W. Zhou, Y. J. Han, G. C. Guo, Phys. Rev. A **74**, 052334 (2006).
  - [4] M. J. Hartmann, F. G. S. L. Brandão, and M. B. Plenio, Laser Photon. Rev. **2**, 527 (2008)
  - [5] M. J. Hartmann, F. G. S. L. Brandão, and M. B. Plenio, Nat. Phys. **2**, 849 (2006).
  - [6] A. D. Greentree, C. Tahan, J. H. Cole, and L. C. L. Hollenberg, Nat. Phys. **2**, 856 (2006).
  - [7] D. G. Angelakis, M. F. Santos, and S. Bose, Phys. Rev. A **76**, 031805 (R) (2007).
  - [8] M. J. Hartmann, F. G. S. L. Brandão, and M. B. Plenio, Phys. Rev. Lett. **99**, 160501 (2007).
  - [9] J. Cho, D. G. Angelakis, and S. Bose, Phys. Rev. A **78**, 062338 (2008).
  - [10] A. C. Ji, X. C. Xie, and W. M. Liu, Phys. Rev. Lett. **99**, 183602 (2007).
  - [11] A. Kay and D. G. Angelakis, Europhys. Lett. **84**, 20001 (2008).
  - [12] D. Rossini and R. Fazio, Phys. Rev. Lett. **99**, 186401 (2007).
  - [13] J. Cho, D. G. Angelakis, and S. Bose, Phys. Rev. Lett. **101**, 246809 (2008).
  - [14] J. Cho, D. G. Angelakis, and S. Bose, Phys. Rev. A **78**, 022323 (2008).
  - [15] Y. Li, M. X. Huo, Z. Song, and C. P. Sun, arXiv:0802.0079.
  - [16] L. Zhou, W. B. Yan, and X. Y. Zhao, J. Phys. B, At. Mol. Opt. Phys. **42**, 065502 (2009)

- [17] S.M. Splillance *et al.*, Phys. Rev. A **71**,013817 (2005).
- [18] K. Hennessy *et al.*, Nature (London) **445**, 896 (2007); B.S. Song *et al.*, Nat. Mater. **4**, 207 (2005).
- [19] A. Wallraff *et al.*, Nature (London) **431**, 162 (2004)
- [20] U. Schollwöck *et al.*, *Quantum Magnetism* (Springer-Verlag Berlin Heidelberg 2004).
- [21] S. Sachdev, *Quantum Phase Transitions* (Cambridge University Press, Cambridge, England, 1999).
- [22] F. D. M. Haldane, Phys. Rev. B **25**, 4925 (1982).
- [23] R. D. Somma and A. A. Aligia, Phys. Rev. B **64**, 024410 (2001).
- [24] J. Zhao, D. X. Yao, S. Li, *et al.*, Phys. Rev. Lett. **101**, 167203 (2008).
- [25] L. Amico, R. Fazio, A. Osterloh and V. Vedral, Rev. Phys. Mod. Phys. **80**, 518 (2008).
- [26] C. M. Dawson, and M. A. Nielsen, Phys. Rev. A **69**, 052316 (2004).
- [27] A. Sen(De), U. Sen, J. Dziarmaga, A. Sanpera, and M. Lewenstein, Phys. Rev. Lett. **101**, 187202 (2008).
- [28] Y. Chen, Z. D. Wang, and F. C. Zhang, Phys. Rev. B **73**, 224414 (2006).
- [29] X. F. Qian, T. Shi, Y. Li, Z. Song and C. P. Sun, Phys. Rev. A **72**, 012333 (2005).
- [30] D. F. V. James and J. Jerke, Can. J. Phys. **85**, 625 (2007).
- [31]  $h_j \approx (\frac{\Omega_1^2}{\Delta_{31}} + \frac{\Omega_4^2}{\Delta_{41}}) - (\frac{\Omega_3^2}{\Delta_{32}} + \frac{\Omega_2^2}{\Delta_{42}}) + \frac{2}{\delta_3}(B_3^2 - A_3^2) + \sum_{p=a,b} \{ \varsigma_{p1} [\frac{1}{\delta_{p1}} (1 + \frac{4J_p^2}{\delta_{p1}^2}) + \kappa_p \frac{2J_p}{\delta_{p1}^2}] + \frac{\varsigma_{p2}}{\delta_{p2}} (1 + \frac{2J_p^2}{\delta_{p2}^2}) \}$ , here,  $\varsigma_{a1} = -A_1^2$ ,  $\varsigma_{b1} = B_1^2$ ,  $\varsigma_{a2} = A_2^2$ ,  $\varsigma_{b2} = -B_2^2$ ,  $\kappa_a = 1$ ,  $\kappa_b = -1$ .
- [32] E. Yusuf and K. Yang, Phys. Rev. B **68**, 024425 (2003).
- [33] S. Bose, Contemp. Phys. **48**, 13 (2007); Z. Song and C. P. Sun, Low Temp. Phys. **31**, 686 (2005).
- [34] Here, local effective magnetic field item is omitted due to the commutation between the XXZ type of Heisenberg interaction and the homogeneous magnetic field.
- [35] M.O. Scully and M.S. Zubairy, *Quantum Optics* (Cambridge University Press, Cambridge, England, 1997).